Polymer 51 (2010) 4860–4866

Contents lists available at ScienceDirect

Polymer

journal homepage: www.elsevier.com/locate/polymer

Mechanism of enhanced tenacity in a polymer nanocomposite studied by small-angle X-ray scattering and electron microscopy

Jayita Bandyopadhyay, Suprakas Sinha Ray*

DST/CSIR Nanotechnology Innovation Centre, National Centre for Nano-Structured Materials, Council for Scientific and Industrial Research, Pretoria 0001, Republic of South Africa

ARTICLE INFO

Article history:
Received 24 March 2010
Received in revised form
8 August 2010
Accepted 17 August 2010
Available online 24 August 2010

Keywords:
Nanocomposite
Improved tenacity
SAXS and TEM

ABSTRACT

A poly[(butylene succinate)-co-adipate] (PBSA) nanocomposite containing 3 wt% organically modified montmorillonite exhibited an improvement in tenacity (elongation at break) as compared to the neat PBSA. The nanocomposite also showed moderate improvement in tensile modulus and strength. The small-angle X-ray scattering and transmission electron microscopy were used to investigate the exact tenacity improvement mechanism in the nanocomposite.

1. Introduction

The mixing of polymer matrices with nanoparticles to form composite materials has been an area of great research interest [1–7]. The mechanical properties of such composite materials are directly related to the properties of the matrix polymer, the properties of the nano-filler, the strength and nature of the interfacial interactions between the polymer matrix and the filler, and finally, the surface area of the interfacial bonds. In the case of nano-filled composite materials, the area of interfacial bond is determined by the aspect ratio of the dispersed particles and the loading level. As the nanoparticles are more nicely dispersed in the polymer matrix, the thickness of the dispersed particles decreases, and as a result the aspect ratio and the affect of the filler on the matrix mechanical properties increase.

One such nanoparticle is clay or more precisely montmorillonite (MMT). MMT is generally ion exchanged with alkyl ammonium or phosphonium cations, known as organically modified MMT (OMMT), to improve the compatibility with engineering polymers. The layer thickness of MMT is around 1 nm, and the lateral dimensions of these layers may vary from 30 nm to several microns or larger, depending on the particular layered silicate [8,9]. The specific surface area of MMT is equal to 750–800 m^2/g, and the modulus of each MMT sheet is around 170 GPa [9]. The true exfoliation of MMT in individual platelets and homogeneous dispersion of uniformly oriented MMT platelets into the polymer matrix will improve the mechanical properties of the composite materials.

Poly[(butylene succinate)-co-adipate] (PBSA) is a synthetic aliphatic polyester and is generally synthesized by the polycondensation of butane-1,4-diol in the presence of succinic and adipic acids with relatively low production cost and satisfactory mechanical properties equivalent to that of polyolefins [10,11]. The PBSA, compared with poly(butylene succinate), is more susceptible to biodegradation because of its lower crystallinity and more flexible polymer chains. It also has excellent processibility, so that in the field of textiles it can be processed into melt-blown, multifilament, monofilament, flat, and split yarns, and in the field of plastics into injection-molded products. It is, thus, a promising polymer for various applications [12].

In recent publications, we have shown that the tensile properties of PBSA increased upon nanocomposite formation with methyl tallow bis(2-hydroxylethyl) quaternary ammonium modified MMT (commercially known as Cloisite® 30B, C30B) [13,14]. During that time we proposed that the high level of interactions between the 'CO' groups on the PBSA backbone with the diols present in the C30B (refer to supporting document) seem to be responsible for the increase in tenacity of the nanocomposites. In this study, we chose a PBSA nanocomposite (PNSANC) containing 3 wt% C30B as a model system to understand the exact mechanism of enhanced tenacity of nanocomposites. The reason for this selection was that recent structural characterizations by small-angle X-ray scattering (SAXS) and transmission electron microscopy (TEM) showed that in

* Corresponding author. Tel.: +27 12 841 2388; fax: +27 12 841 2229.
E-mail address: rsuprakas@csir.co.za (S. Sinha Ray).

0032-3861/$ – see front matter © 2010 Elsevier Ltd. All rights reserved.
doi:10.1016/j.polymer.2010.08.040

the case of PBSANC3 silicate layers have enough available space to orient themselves in the PBSA matrix [15]. It is well established that the final properties of a nanocomposite are directly related to the dispersion characteristic and orientation of the silicate layers in the polymer matrix. For this reason, detail structural analyses of neat polymer and nanocomposite injection-molded samples, before and after tensile tests, were characterized by SAXS combined with bright-field TEM to find out the exact mechanism of enhanced tenacity in the case of the nanocomposite.

2. Experimental procedure

2.1. Materials and preparation of the nanocomposite

The PBSA used in this study is a commercial product from Showa High polymer (Japan), with the designation BIONOLLE #3001. Organoclay used in this study was C30B, purchased from Southern Clay Products. Detailed information about PBSA and C30B can be found in the supporting document. The PBSANC containing 3 wt% of C30B (abbreviated as PBSANC3) was prepared in a Polylab Thermohaake-batch mixer at 135 °C and a rotor speed of 60 rpm for 8 min. The dried neat PBSA and nanocomposite strands were injection-molded using an injection-molding machine (bench-top Haake Minijet II) operated at 135 °C with a mold temperature of 60 °C (ASTM D-638). Neat PBSA and PBSANC3 samples were annealed at 50 °C under vacuum prior to all characterizations and property measurements.

2.2. Characterization techniques

The tensile modulus, tensile strength, and elongation at break were measured in a tensile Instron 88215 tester (load 5 kN) with a cross-head speed of 5 cm/min. The data presented here are the mean of eight independent tests. Experiments were conducted after being conditioned in the laboratory environment, temperature 25 °C and relative humidity 40%. SAXS experiments were carried out by an Anton Paar SAXSess instrument, operated at 40 kV and 50 mA using a point collimation geometry. The radiation used was a CuK_{α} radiation, with a wavelength of 0.154 nm (PAN Analytical X-ray source). Intensity profiles were obtained with a point collimated SAXSess and recorded with a two-dimensional (2D) imaging plate. The sample-to-detector distance was 264.5 mm and covered the length of the scattering vector (q) from 0 to 16 nm^{-1}. The read-out angles were calculated from the pixel size, and the obtained q-scale was cross-checked by measuring silver behenate whose equidistant peak positions are known. SAXS data were collected at room temperature, and all samples were exposed under X-ray for 1 h. The thickness of the samples varied roughly between 0.6 and 0.9 mm, and was collected from injection-molded bars as described in Fig. 1. The dispersion characteristic of the layered silicate particles in PBSA matrix before and after the tensile tests was investigated by means of a high-resolution TEM (JEOL JEM2100), operated at an accelerating voltage of 100 kV. The ultra-thin sections (Fig. 1) with a thickness of 100 nm were microtomed at −80 °C using a Reichert Ultracut cryo-ultramicrotome without staining.

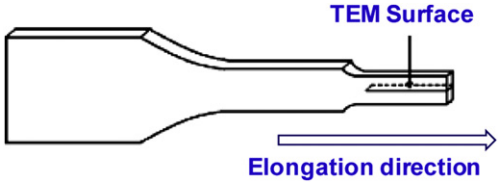

Fig. 1. Sample surface used for TEM analysis.

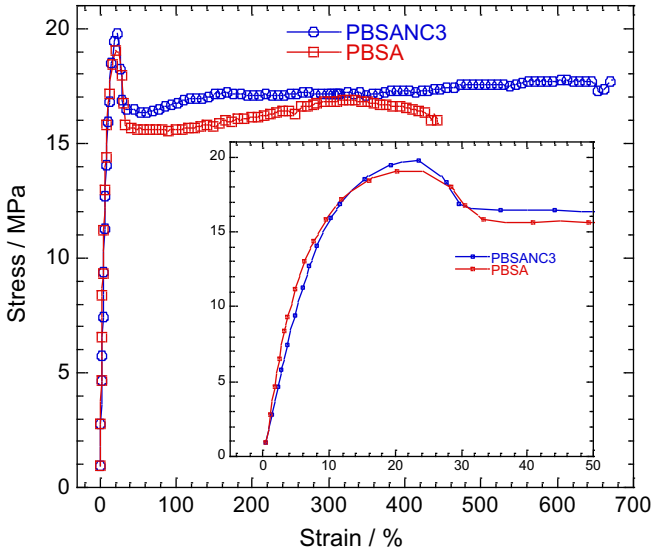

Fig. 2. Typical stress–strain curves of annealed injection-molded neat PBSA and PBSANC3 (containing 3 wt% C30B) samples.

3. Results and discussion

The typical stress–strain curves for neat PBSA and PBSANC3 are given in Fig. 2, and their tensile properties are presented in Table 1. The tensile modulus value of neat PBSA is ~200 MPa, and this value place PBSA in a very different category, something just beyond the stiff rubbers. The modulus of PBSANC3 is ~28% higher than that of neat PBSA, and the yield strength of PBSANC3 increases by 19% in comparison to the neat PBSA. On the other hand, compared to the neat PBSA matrix, tenacity of PBSANC3 increases by 50%. Based on the enthalpy of melting, a previous study showed that the crystallinity of PBSA matrix slightly decreases upon nanocomposite formation with C30B. The degree of crystallinity decreased from ~48% for neat PBSA to ~42% for PBSANC3 [11,16,17]. Such a slight decrease in crystallinity cannot solely explain the significant improvement in the tenacity of the nanocomposite. To have a better understanding into the increased tenacity of the nanocomposite, SAXS analyses of injection-molded neat PBSA and nanocomposite samples, before and after tensile tests, were carried out in detail.

In a densely packed system of particles, the positional ordering can develop a preferential orientation with respect to each other, especially when the particles are not spherical. The degree of orientation can be detected easily from the 2D SAXS patterns. An arc-profile is usually used to determine the orientation of crystals in a certain basal plane. Parts (a) and (b), respectively, of Fig. 3 represent the 2D SAXS patterns of PBSA and PBSANC3 before the tensile test. Similarly, the 2D SAXS patterns of PBSA and PBSANC3 after the tensile tests are shown in parts (c) and (d), respectively, of Fig. 3. According to Fig. 3(a) and (b), neither PBSA nor PBSANC3 possesses any preferred orientation in the masked crystal plane. But after the tensile test (Fig. 3(c) and (d) both PBSA and PBSANC3 show scattering patterns similar to the oriented sample. The scaled normalized scattering profiles (determined on the basis of the arc-mask as shown in Fig. 3) against the orientation angle for all samples are presented in Fig. 4. Again, the degree of anisotropy

Table 1
Tensile properties of neat PBSA and PBSANC3 (containing 3 wt% of C30B) samples.

Sample	Modulus/MPa	Yield strength/MPa	Tenacity/%
PBSA	213.2 ± 9	16.7 ± 0.8	440 ± 8
PBSANC3	272.1 ± 15	20.0 ± 1.0	660 ± 7

The data presented here are means of eight individual tests.

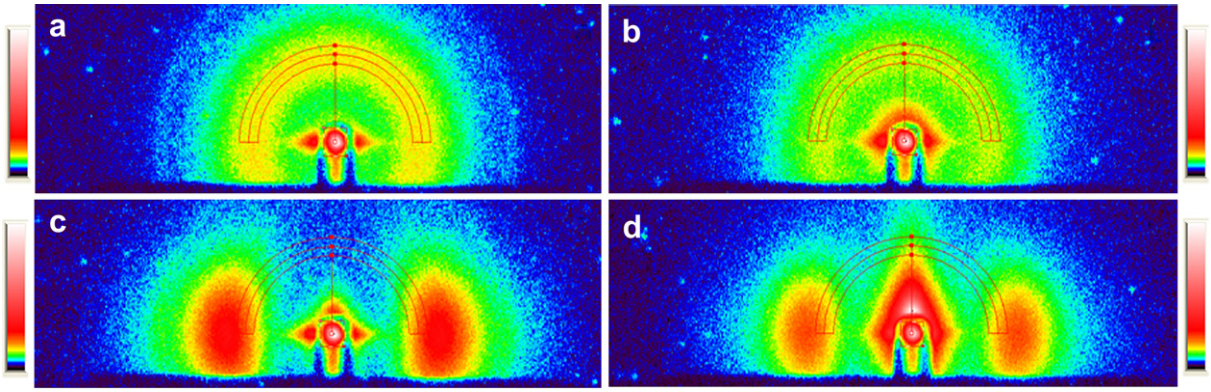

Fig. 3. Two-dimensional small-angle X-ray scattering patterns: (a) PBSA before the tensile test, (b) PBSACN3 before the tensile test, (c) PBSA after the tensile test, and (d) PBSANC3 after the tensile test. SAXS samples were prepared according to the Fig. 1 and for all samples; the contrast was kept at 53 during determination of the arc-profile.

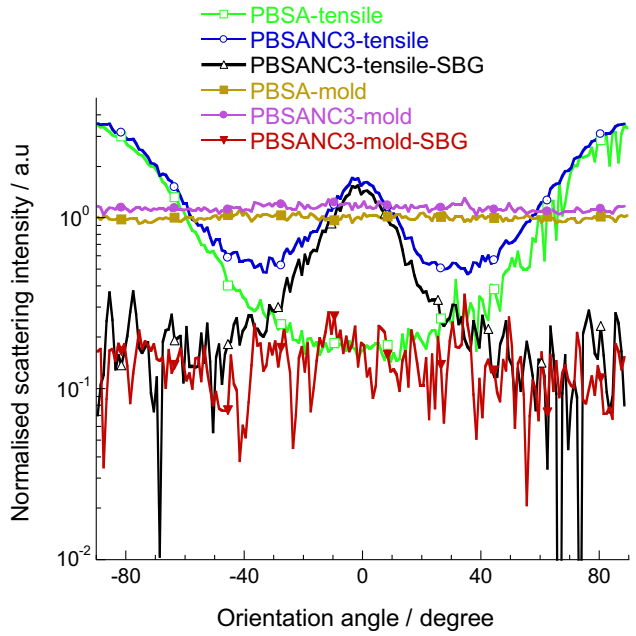

Fig. 4. The scaled normalized scattering profiles (determined on the basis of the arc-mask as shown in Fig. 3) against the orientation angle. Mold indicates molded sample; tensile indicates after tensile test; and SBG indicates background (here PBSA) subtracted.

(DOA) and the mean orientation angle from the azimuthal scattering profiles (Fig. 4) were estimated using the 'TDOA' program and calculated values are presented in Table 2. The TDOA program uses the following equations to evaluate d and the mean orientation angle from azimuthal scattering profiles [18,19].

A point on the azimuthal scan can be presented by a unit vector, u, such that $u_1 = \cos\beta$ and $u_2 = \sin\beta$, where β is the azimuthal angle. The anisotropy in the X-ray scattering pattern can be obtained by the weighted average of the second moment tensor of 'u' as

$$\langle uu\rangle = \begin{bmatrix} \langle u_1u_1\rangle\langle u_1u_2\rangle \\ \langle u_1u_2\rangle\langle u_2u_2\rangle \end{bmatrix} = \begin{bmatrix} \langle \cos^2\beta\rangle\langle \sin\beta\cos\beta\rangle \\ \langle \sin\beta\cos\beta\rangle\langle \sin^2\beta\rangle \end{bmatrix} \quad (1)$$

Here, $<\ldots>$ represents an average weighted by the azimuthal intensity distribution and $<\cos^2\beta>$ can be expressed as

$$\left\langle \cos^2\beta \right\rangle = \frac{\int_0^{2\pi} \cos^2\beta I(\beta)\mathrm{d}\beta}{\int_0^{2\pi} I(\beta)\mathrm{d}\beta} \quad (2)$$

The difference in eigenvalues $(\lambda_1 - \lambda_2)$ of $<uu>$ gives a measure of the anisotropy factor and can be expressed as

$$\lambda_1 - \lambda_2 = \sqrt{(\langle u_1u_1 - u_2u_2\rangle)^2 + 4\langle u_1u_2\rangle^2} \quad (3)$$

The degree of anisotropy determined by the TDOA program is $(\lambda_1 - \lambda_2)$ in percent.

Table 2
The degree of anisotropy and the mean orientation angle were calculated from the azimuthal scattering profiles.

Sample[a]	Orientation angle/ degree	Degree of anisotropy/%	Symmetry/ fold
PBSA-tensile	90	74.8	2
PBSANC3-tensile-SBG	−2.4	42.9	2

[a] SBG, background (PBSA) subtracted.

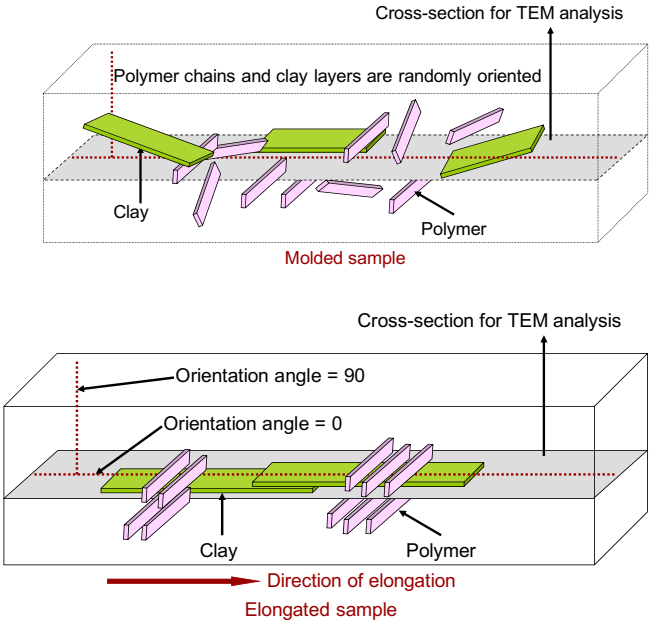

Fig. 5. Schematic representations of the orientation of polymer chains and dispersed silicate layers before and afterl the tensile tests.

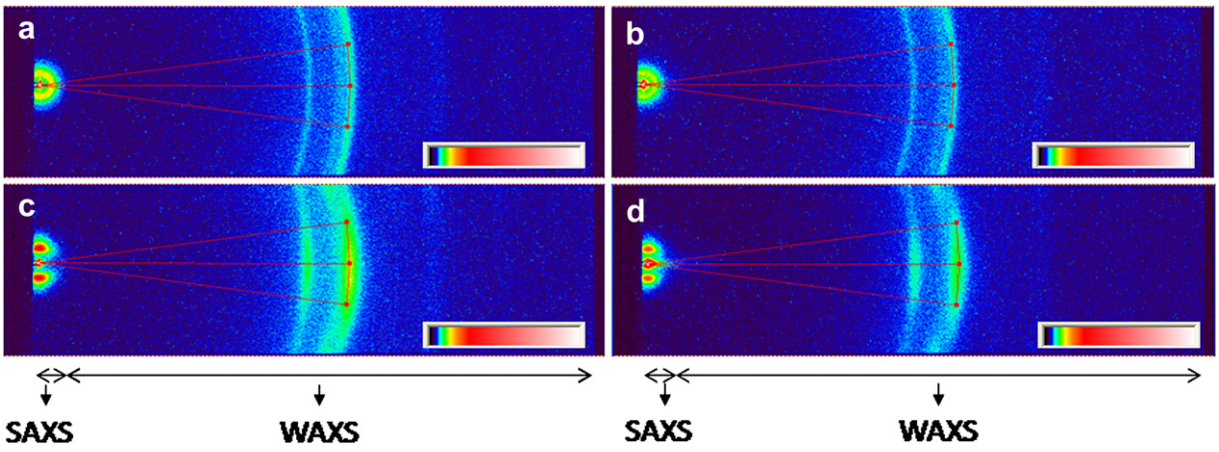

Fig. 6. Two-dimensional (2D) small-and wide-angle X-ray scattering (SWAXS) patterns of various samples with pi-profiles: (a) PBSA sample before the tensile test, (b) PBSANC3 before the tensile test, (c) PBSA sample after the tensile test, and (d) PBSANC3 sample after the tensile test. Samples were prepared according to Fig. 1.

The mean orientation angle or the average domain orientation angle can be expressed as

$$\overline{\chi} = \frac{1}{2}\tan^{-1}\left(\frac{2\langle u_1 u_2\rangle}{\langle u_1 u_1\rangle - \langle u_2 u_2\rangle}\right) \quad (4)$$

Fig. 4 shows that the molded PBSA and PBSANC3 samples do not possess a specific orientation since the normalized intensity remains constant throughout the range of the orientation angles. However, according to Table 2 and Fig. 4, after the tensile test the neat PBSA chains exhibit an orientation at ±90°. On the other hand, in the case of the PBSANC3, three intensity maxima appear (at ±90° and −2.4°) in the azimuthal scattering profile (Fig. 4). The resultant profile (PBSANC3-tensile-SBG) obtained after subtraction of the PBSA profile from the PBSANC3 confirms the orientation ~ −2.4° (Table 2) is due to the oriented dispersed clay particles in the PBSA matrix.

The schematic diagrams of the orientation of the polymer chains and the dispersed silicate layers before and after the tensile tests are presented in Fig. 5. In this figure, the polymer chains are denoted by the pink blocks and clay particles by the green blocks. If we now consider the orientation of the polymer chains and clay layers on the surface parallel to the direction of elongation, before the tensile test both polymer chains and clay layers are randomly oriented. Again, if we consider that the zero-angle position is in the direction of elongation, one can infer that the clay layers become oriented almost in the direction of applied strain during the tensile test, and the polymer chains arrange themselves orthogonally to the clay surfaces. According to Fig. 5, the orientation of polymer chains remains the same in PBSA-tensile and PBSANC3-tensile, and they are attaining the same intensity values at an orientation angle of ±90°. Therefore, one can expect that the anisotropy factor due to the polymer chains remains the same in PBSA-tensile and PBSANC3-tensile. According to Table 2, the degree of anisotropy for PBSA-tensile is 74.8%. The PBSANC3-tensile-SBG provides information about the extra anisotropy induced by the clay particles in the nanocomposite and it is 42.9%. Therefore, since the anisotropy increases in the case of PBSANC3, it is expected that the anisotropically dispersed clay particles will offer a large interfacial region that provides a convenient mechanism for energy dissipation. As a result, the elongation at break (or tenacity) increases in PBSANC3 compared to the neat PBSA as obtained in Fig. 2. Again, according to Table 2, PBSA-tensile and PBSANC3-tensile-SBG systems possess a two-fold rotational symmetry for the azimuthal scattering pattern. The two-fold rotational symmetry means the intensity profile has a period of 180°.

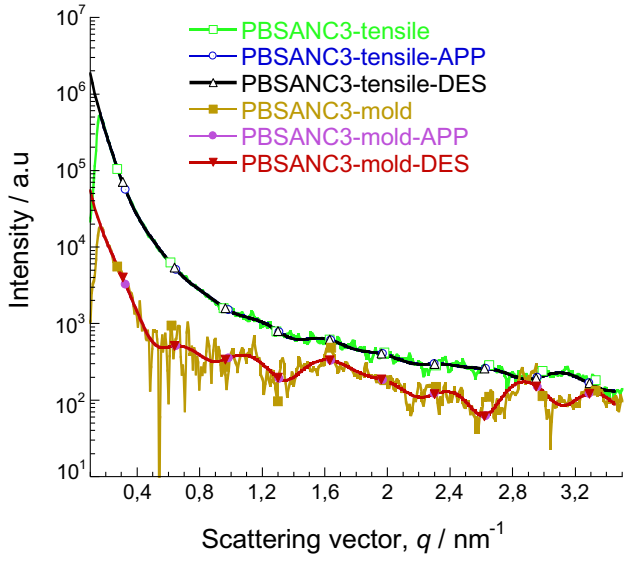

Fig. 7. Background (here PBSA) subtracted scattering profile of various nanocomposite (PBSANC3) samples. DES stands for desmeared scattering curves, APP stands for approximated scattering curves determined on the basis of GIFT. The term tensile indicates sample after the tensile test and mold indicates injection-molded sample.

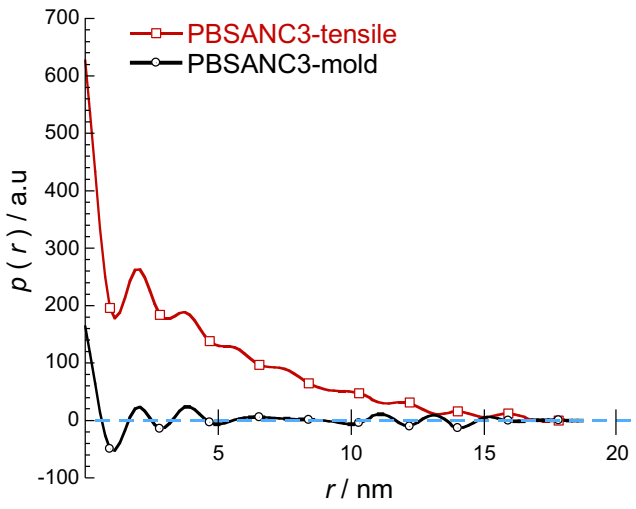

Fig. 8. The pair-distance distribution functions, $p(r)$ for nanocomposite (PBSANC3) before (PBSANC3-mold) and after (PBSANC3-tensile) the tensile tests.

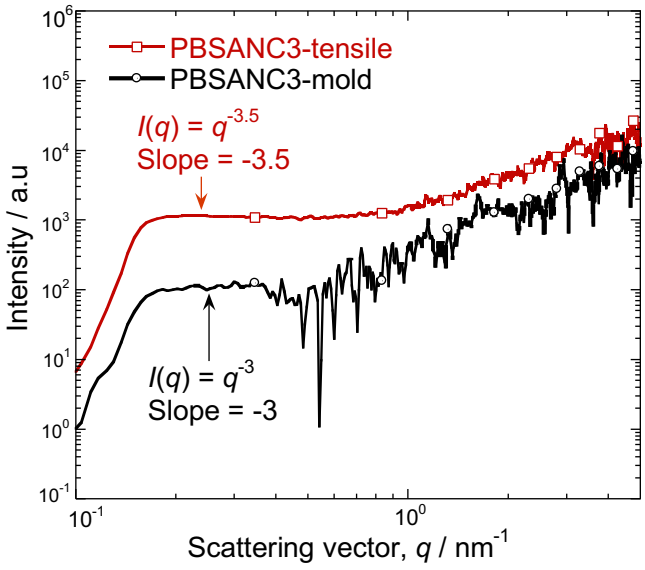

Fig. 9. Power law verifications on nanocomposite (PBSANC3) sample before (PBSANC3-mold) and after (PBSANC3-tensile) the tensile tests. Background-subtracted scattering curves were used.

It is now clear from the above discussion that in the molded nanocomposite sample the clay particles are oriented isotropically (that is, randomly oriented), whereas after the tensile tests they orient themselves in the direction of applied tensile strain. It is expected that this change in orientation should affect the dispersion characteristics of the clay platelets in the polymer matrix. Now to investigate this, the pi-profile is used to analyse the same 2D SAXS patterns with the same contrast as before. The 2D images with pi-profiles are presented in Fig. 6. The parts (a) and (b) of Fig. 6 represent, respectively, the 2D images of the molded PBSA and PBSANC3 samples and parts (c) and (d) represent, respectively, the 2D images of the PBSA and PBSANC3 samples after the tensile tests. Now the PBSA profile (obtained on the basis of the 2D image) is subtracted from the scaled PBSANC3 profile before and after the tensile tests to get information about the dispersed clay particles in both states. The results are reported in Fig. 7 as PBSANC3-mold and PBSANC3-tensile. Theses two curves were analyzed according to the Generalized Indirect Fourier Transformation (GIFT) technique as illustrated in the supporting document. According to this technique, the sum of the Fourier Transformed spline functions whose oscillations are restricted by Lagrange multipliers (λ_L) gives an approximated desmeared scattering curve. After incorporation of the slit collimation effect it gives an approximated scattering curve that matches nicely with the experimental scattering curve and also provides $p(r)$. $p(r)$ is the pair-distance distribution function of the electrons; in other words, the radial or spherical symmetric correlation function of electron density differences weighted by $4\pi r^2$. It shows directly the probability of finding a pair of electron densities at a particular distance r. As mentioned in the illustration of the GIFT technique, it requires the specification of the number of spline functions (N) and the upper limit of the largest particle dimension (D_{max}). The number of spline functions (N) used to cover the range of $p(r)$ was 20, and D_{max} for PBSANC3 before and after the tensile test was 18.7 nm. Initially, we determined the approximated scattering curve, $I_A(q)$, for 19 different λ_L-values, and, finally, we choose a particular λ_L-value for which $I_A(q)$ is almost similar to the experimental scattering curve, $I_{exp}(q)$. In Fig. 7 APP and DES stand for approximated and desmeared scattering curves, respectively, and the curves without any extension represent the experimental scattering curve, $I_{exp}(q)$. Fig. 7 shows that the approximated results are matching nicely with the experimental scattering curve. Therefore, the approximated pair-distance distribution function of the electrons, $p_A(r)$, from where $I_A(q)$ was estimated should be similar to the $p(r)$ representing $I_{exp}(q)$. The $p(r)$ of PBSANC3 before and after the tensile test is presented in Fig. 8. The regions with opposite signs of different electron density give negative contributions to $p(r)$; that is $p(r)$ can be negative in some regions as observed for the case of the PBSANC3-mold in Fig. 8. The correlation maximums (that is, the peak positions) represent the average radial distance to the next neighboring domain, commonly known as long spacing. When the neighbors overlap, the peaks don't possess a tail; rather, a curve shows a maxima and minima. Therefore, in the PBSANC3-mold stacked clay layers are mostly separated. After the tensile test the stacked clay layers orient in the direction of the applied strain in such a way that the clay layers start to overlap, and hence the distribution $p(r)$ is changing in the case of the PBSANC3-tensile sample. Therefore, according to Fig. 8, the PBSANC3-mold sample possesses some distinct neighbors along with a few overlapping in the range of 5–10 nm. On the other hand, the PBSANC3-tensile sample possesses eight neighbors overlapping on each other, and hence there is no negative contribution of electron density to $p(r)$.

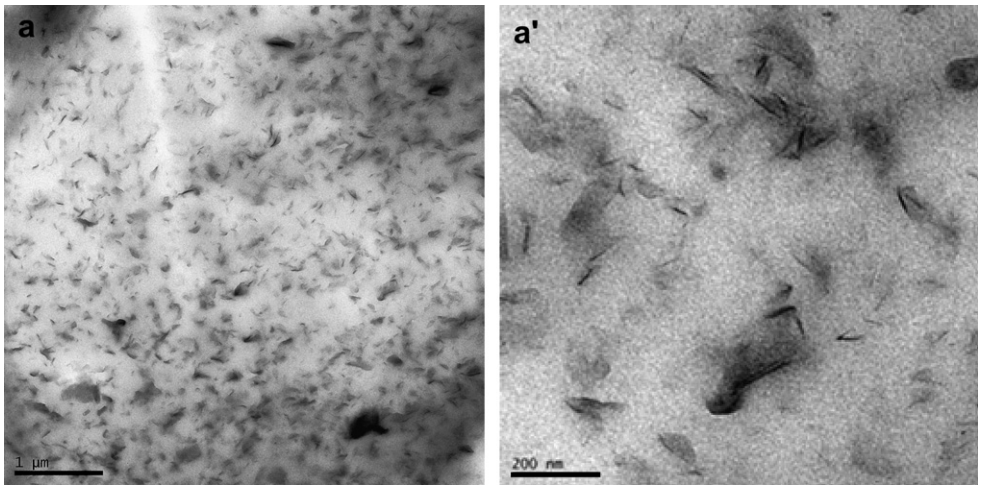

Fig. 10. (a, a′) Bright-field TEM image of injection-molded nanocomposite sample at two different magnifications. TEM sample was prepared according to Fig. 1.

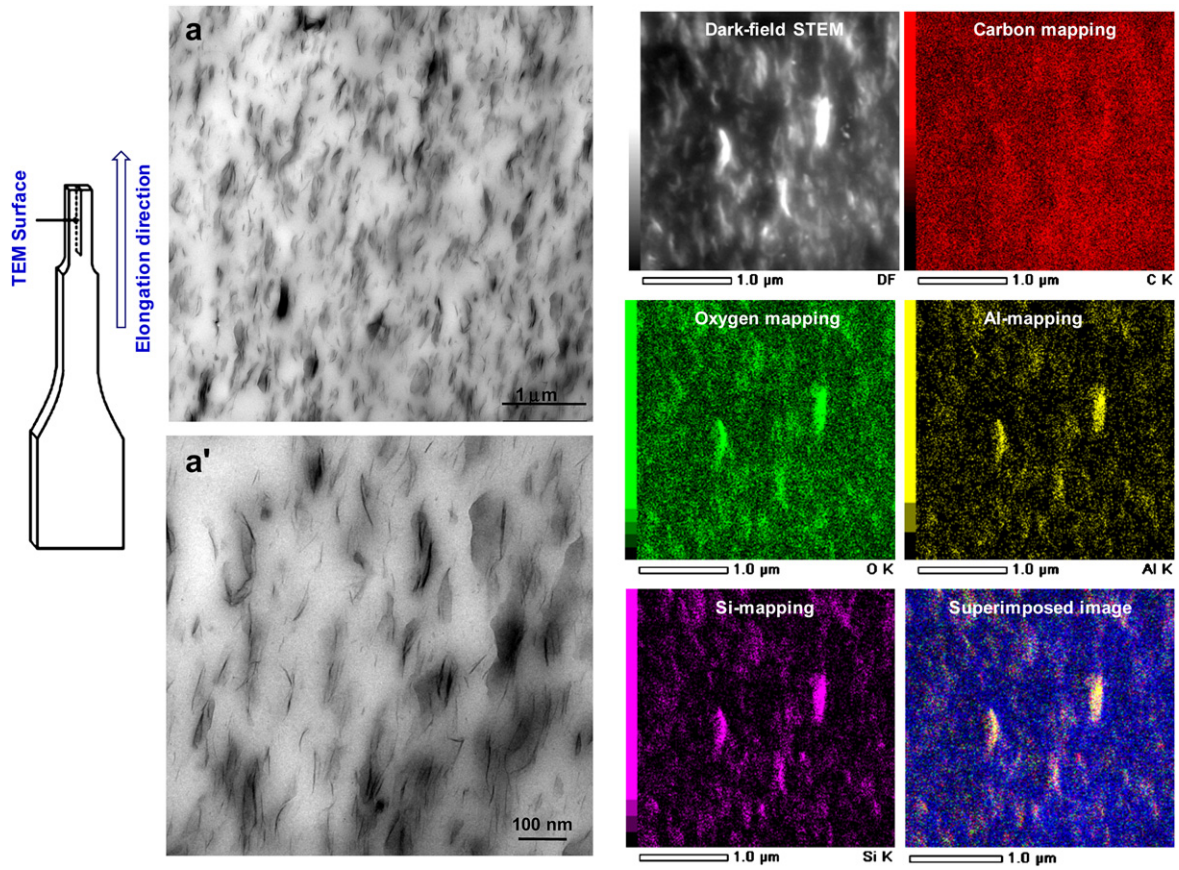

Fig. 11. (a, a′) Bright-field TEM image of nanocomposite sample after tensile test and (b) X-ray mapping of various elements in scanning transmission electron microscopy mode. This result shows silicate layers are oriented towards the direction of applied strain.

The power law for the PBSANC3-mold and PBSANC3-tensile samples are presented in Fig. 9. Ideally, in the case of monodisperse exfoliated lamellae the slope should be −2 and for spherical particles it should be −4. Here, for the PBSANC3-mold and -tensile samples, the slopes are −3 and −3.5, respectively. Such an observation indicates that the clay lamellae are thick; that is, they are sticking together in the case of both samples. However, they are not thick enough to form globules. Since the overlapping increases in the case of the PBSANC3-tensile sample compared to the molded sample, the slope decreases in the case of PBSANC3 sample after the tensile test.

To support the conclusions based on the SAXS results, the molded nanocomposite samples before and after the tensile test were investigated by TEM because microscopy allows an understanding of the internal structure through direct visualization. Fig. 10 shows the most representative bright-field TEM images of the PBSANC3-molded sample before the tensile test. It is clear from the image that clay particles are randomly oriented in the PBSA matrix. The TEM images of the PBSANC3 sample at two different magnifications after the tensile test are presented in Fig. 11(a, a′), which clearly show that the clay particles are much thicker compared to that of the molded sample and are nicely oriented in the direction of the tensile strain. Such observations were further supported by the X-ray elemental mapping in the scanning transmission mode, Fig. 11(b). Therefore, TEM results are in good agreement with the SAXS results as discussed above.

4. Conclusions

The detail structural analyses of neat polymer and nanocomposite samples, before and after the tensile test, were carried out to understand the exact mechanism responsible for the enhanced elongation at break of the nanocomposite sample. Results showed that the enhanced tenacity in the case of the nanocomposite is due to the orientation of the dispersed clay layers in the direction of the applied tensile strain. Further, this orientation affects the dispersion characteristics in such a way that the clay layers overlap. This allows a better energy-dissipation mechanism which in turn is responsible for the concurrent improvement in tensile properties.

Acknowledgements

The authors would like to thank the CSIR executive and the DST, South Africa, for financial support.

Appendix. Supplementary data

Supplementary data associated with this article can be found in the online version, at 10.1016/j.polymer.2010.08.040.

References

[1] Pavlidou S, Papaspyrides CD. A review on polymer-layered silicate nanocomposites. Prog Polym Sci 2008;33:1119–98.
[2] Paul DR, Robeson LM. Polymer nanotechnology: nanocomposites. Polymer 2008;49:3187–204.
[3] Sinha Ray S, Bousmina M. Biodegradable polymers and their layered silicate nanocomposites: in greening the 21st century materials world. Prog Mater Sci 2005;50:962–79.
[4] Sinha Ray S, Okamoto M. Polymer/layered silicate nanocomposites: a review from preparation to processing. Prog Polym Sci 2003;28:1539–41.
[5] Alexandre M, Dubois P. Polymer-layered silicate nanocomposites: preparation, properties, and use of a new class of materials. Mater Sci Eng 2000;R28:1–63.

[6] Lloyd SM, Lave LB. Life cycle economic and environmental implications of using nanocomposites in automobiles. Environ Sci Eng 2003;37:3458–66.
[7] Sinha Ray S, Makhatha ME. Thermal properties of poly(ethylene succinate) nanocomposite. Polymer 2009;50:4635–43.
[8] Klimentidis RE, Mackinnon IDR. High-resolution imaging of ordered mixed-layer clays. Clays Clay Miner 1986;34:155–64.
[9] (a) Grim RE. Clay mineralogy. New York: McGraw-Hill; 1953;
(b) Pinnavaia TJ. In: Legrand AP, Flandrois S, editors. Chemical physics of intercalation. New York: Plenum; 1987.
[10] Ishioka D. Biopolymers, polyesters III. Applications and commercial products, vol. 4. Weinheim: Wiley-VCH Verlag Gmbh; 2002. p. 275.
[11] Nikolic MS, Djonlagic J. Synthesis and characterization of biodegradable poly [(butylene sucinate)-co-adipate]s. Polym Degrad Stab 2001;74:263–70.
[12] Fujimaki T. Processability and properties of aliphatic polyesters, 'BIONOLLE', synthesized by polycondensation reaction. Polym Degrad Stab 1998;59:209–14.
[13] Sinha Ray S, Bousmina M. Poly[(butylene sucinate)-co-adipate]/montmorillonite nanocomposites: effect of organic modifier miscibility on structure, properties, and viscoelasticity. Polymer 2005;46:12430–9.
[14] Sinha Ray S, Bousmina M. Structure and properties of nanocomposites based on poly[(butylene succinate)-co-adipate] and organically modified montmorillonite. Macromol Mater Eng 2005;290:759–68.
[15] Bandyopadhyay J, Sinha Ray S. The quantitative analysis of nano-clay dispersion in polymer nanocomposites by small-angle X-ray scattering combined with electron microscopy. Polymer 2010;41:1437–49.
[16] Bandyopadhyay J, Maity A, Khatua BB, Sinha Ray S. Thermal and rheological properties of biodegradable poly[(butylene succinate)-co-adipate] nanocomposites. J Nanosci Nanotechnol 2010;10:4184–95.
[17] Sinha Ray S. A new possibility for microstructural investigation of clay-based polymer nanocomposite by focused ion beam tomography. Polymer 2010;51:3966–70.
[18] Cinader JR, Burghardt WR. X-ray scattering studies of orientation in channel flows of a thermotropic liquid-crystalline polymer. J Polym Sci Part B Polym Phys 1999;37:3411–28.
[19] Caputo FE, Burghardt WR. Real-time 1–2 plane SAXS measurements of molecular orientation in sheared liquid crystalline polymers. Macromolecules 2001;34:6684–94.